Wind and Structures, *Vol. 18, No. 2 (2014) 135-154*
DOI: http://dx.doi.org/10.12989/was.2014.18.2.135

Aerodynamic force characteristics and galloping analysis of iced bundled conductors

Wenjuan Lou[1], Jiang Lv[1], M.F. Huang[*1], Lun Yang[1] and Dong Yan[2]

[1]*Institute of Structural Engineering, Zhejiang University, Hangzhou, 310058, Zhejiang, China*
[2]*Henan electric power testing and research institute, Zhenzhou, 450052, Henan, China*

(Received May 23, 2013, Revised September 13, 2013, Accepted October 15, 2013)

Abstract. Aerodynamic characteristics of crescent and D-shape bundled conductors were measured by high frequency force balance technique in the wind tunnel. The drag and lift coefficients of each sub-conductor and the whole bundled conductors were presented under various attack angles of wind. The galloping possibility of bundled conductors is discussed based on the Den Hartog criterion. The influence of icing thickness, initial ice accretion angle and sub-conductor on the aerodynamic properties were investigated. Based on the measured aerodynamic force coefficients, a computationally efficient finite element method is also implemented to analyze galloping of iced bundled conductors. The analysis results show that each sub-conductor of the bundled conductor has its own galloping feature due to the use of aerodynamic forces measured separately for every single sub-conductors.

Keywords: iced bundled conductors; aerodynamic force coefficients; galloping analysis; wind tunnel tests

1. Introduction

Galloping of iced conductors is a self-excited vibration with high amplitude and low frequency (Ohkuma and Marukawa 2000, Guo *et al*. 2002). Transmission line galloping may bring wear and damages to the conductors, the fittings and the tower components. The frequent occurrence of galloping seriously affects the reliability of electric power transmission and causes significant economic losses. Den Hartog (1932) and Nigol and Buchan (1981) are among the pioneers who studied the galloping mechanisms and proposed some criteria for the onset of galloping. Van Dyke and Laneville (2008) carried out a field test on the galloping of a single conductor covered with a D-section. It has been demonstrated that wind attack angle may strongly influence the galloping amplitude. The effectiveness of interphase spacers on galloping reduction were also studied by field tests. With the rapid development of computational fluid dynamics (CFD) technique, it becomes feasible to carry out numerical simulation for aerodynamic problems of bluff body. LV *et al*. (2010) performed a numerical simulation to acquire aerodynamic characteristics of 3-bundled conductors in crescent and fan-shape. The good agreement of aerodynamic force coefficients between numerical simulation and experimental test has been found in the work.

∗Corresponding author, Associate Professor, E-mail: mfhuang@zju.edu.cn

http://www.techno-press.org/?journal=was&subpage=8 ISSN: 1226-6116 (Print), 1598-6225 (Online)

Compared to field measurements and numerical simulation, wind tunnel test still play a dominant role in quantifying the aerodynamic force parameters of iced conductors. Chabart and Lilien (1998) measured the quasi-static aerodynamic coefficients for different wind speed in the range of galloping observations. Shimizu *et al*. (2004) carried out a wind tunnel study of single and four-bundled conductors with specific accreted ice shapes. The findings show that the drag and lift coefficient of single conductor almost consistent with that of 4-conductor bundle. But the moment coefficient does not agree with between single conductor and 4-conductor bundle owing to the wake effects from upstream conductors. Xiao *et al*. (2009) made use of icing wind tunnel to investigate aerodynamic characteristics of 8-bundled conductors artificially iced in the wind tunnel.

The significant interference effects among sub-conductors were found. Gu *et al*. (2009) studied aerodynamic force characteristics and stabilities of two typical iced conductors by tests on their rigid section models using high frequency balance technique in wind tunnel. Wang *et al.* (2011) conducted a wind tunnel test to obtain the aerodynamic coefficients of crescent and D-shape single conductors. Uniform flow and homogeneous turbulence flow were both used in the test to investigate the influences of turbulence on the aerodynamic characteristics of iced conductors. The comprehensive experimental investigation using aeroelastic cable models were recently reported by Li *et al*. (2013). It was observed that wake galloping of parallel stay cables is sensitive to the angle of attack.

Although many efforts have been made to acquire the aerodynamic force coefficients of iced conductors, a systematic study on a series of test models is still lacking. Aerodynamic force coefficients of iced conductors under varying wind angles are closely related to their galloping behaviors. Barrro *et al*. (2009) reveals the existing link between the hysteresis phenomenon of galloping and the number of inflection points at the aerodynamic force coefficient curve. More wind tunnel studies are needed to collect adequate aerodynamic force coefficient data of bundled conductors with various numbers of sub-conductors in two common ice shapes, i.e., crescent and D-shape.

Once the aerodynamic forces on the iced conductors are determined from the wind tunnel experiments, the next task is to carry out the analysis of cable galloping, which is a typical aerodynamic and geometric nonlinear problem with the characteristics of small strain and large displacement. Many researchers have made efforts to study and develop galloping analysis methods (Yu *et al*. 1992, Desai *et al*. 1995, Macdonald and Larose 2006, Sun and Lou 2010, Wang and Lou 2010, Raeesi *et al*. 2013). Two main approaches are employed to perform galloping analysis. One is analytical approach by developing various analytical models, including a single-degree-of-freedom (DOF) vertical plunge model (Den Hartog 1932, Parkinson 1989), 2DOF model (Yu *et al*. 1992, Jones 1992), and 3DOF model to consider torsion (Yu *et al*. 1993). From these analytical models, approximate solutions and stability conditions can be expressed explicitly in terms of known system's parameters. Very recently, Raeessi *et al*. (2013) proposed a quasi-steady analytical model to study the aerodynamic damping ratio of an inclined circular cable oscillating in unsteady flow, with practical application to predict divergent galloping type of response on bridge stay cables. The other approach is based on finite element numerical modeling method (Desai *et al*. 1995, Luongo *et al*. 2008, 2009, Yan *et al*. 2013). A finite element based model, in conjunction with a time-step algorithm, can easily accommodate various component interactions as well as the effects of nonlinearity. Based on the curved-beam theory, Yan *et al*. (2013) developed one nonlinear numerical analysis method for galloping of iced transmission line, with regard of bending stiffness of the transmission line and eccentricity of accreted ice.

This paper presents main results based on a series of wind tunnel tests for iced bundled conductors. The possibility of galloping and the range of attack angle which galloping can occur were analyzed based on the Den Hartog theory. The effects of three major factors, i.e., the ice thickness, the initial ice accretion angle and interference among sub-conductors, on aerodynamic characteristics and galloping behavior of iced bundled conductors were investigated. Finally, the measured aerodynamic coefficients were used in the galloping analysis of a practical transmission line for ultra high-voltage (UHV) grids by the finite element method (FEM). The transmission line consists of iced 6-bundled conductors linked with spacers, which were numerically modeled by a three-node parabolic conductor element and Euler beam element, respectively.

2. Wind tunnel tests

2.1 Test models

The appearance of iced conductor is influenced by many factors, such as meteorological condition, local topographic and the layout of transmission lines. When the weather condition is in low temperature, gentle wind and light rain, the ice shape tends to be crescent as the drop freezes immediately. If the temperature increases and the rain become heavy, the ice shape becomes D-shape due to the delay of freezing and wind separation along the windward of the conductor. Therefore, the crescent and D-shape were chosen as two typical accreted ice shapes in this study. Sectional rigid models of iced conductors with varying sizes were fabricated in a full scale dimension. The diameter (D) of crescent conductor was taken as 26.8 mm, and the ice thickness were taken as 0.25D, 0.5D, 0.75D and 1.0D, respectively. The D-shape conductor model was prepared with the conductor diameter of 23.9mm and the ice thickness of 23 mm. All of the models were 800 mm in length and made of glass fiber reinforced plastics. Fig. 1 shows the pictures of the crescent and D-shape iced conductor models and their cross sections.

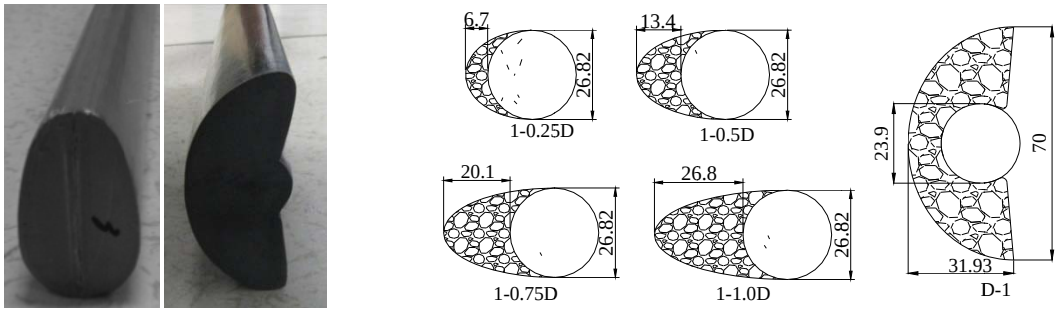

Fig. 1 Rigid section models and their sizes

2.2 Test cases

In order to investigate the effect of ice thickness on the aerodynamic properties of bundled conductors, four cases with varying ice thickness from 0.25 D to D (as listed in Table 1) were

tested for four-bundled crescent conductors. The definition of aerodynamic force components and wind angle of attack for four-bundled crescent iced conductors is given in Fig. 2.

According to CIGRE (2005), the initial ice accretion angle is defined as the initial ice position on the conductor. A deposit of ice upon the conductor could lend it suitable aerodynamic characteristics, and the position of that ice deposit (initial ice accretion angle) together with a certain wind angle could favor aerodynamic instability. Initial ice accretion angle is an important parameter to study aerodynamic stability of iced conductors, and is influenced by temperature, wind condition and the torsional stiffness of conductor. The dangerous ice accretion angle can be identified by studying different possible static position of the iced bundled conductors. However, there is lacking of adequate studies to reveal the effects of initial ice accretion angle on aerodynamic characteristics of iced conductors. Four initial ice accretion angles, i.e., 30°, 45°, 60° and 75°, were considered for both two-bundled and six-bundled D-shaped conductor models resulting in eight testing cases (numbered as case 5 to case 12 in Table 1). Eight configurations of test models with varying initial ice accretion angle were given in Fig. 3.

Table 1 Tests cases and the specifications of the models

Num	Ice shape	Number of conductors	Conductor space/mm	Conductor diameter/mm	Thickness of ice/mm	Initial ice accretion angle /°	Conductor tested
1	Crescent	4-bundled	450	26.8	6.7	0	Whole
2	Crescent	4-bundled	450	26.8	13.4	0	Whole
3	Crescent	4-bundled	450	26.8	20.1	0	Whole
4	Crescent	4-bundled	450	26.8	26.8	0	Whole
5	D-shape	2-bundled	448	23.9	23.1	30	Whole
6	D-shape	2-bundled	448	23.9	23.1	45	Whole
7	D-shape	2-bundled	448	23.9	23.1	60	Whole
8	D-shape	2-bundled	448	23.9	23.1	75	Whole
9	D-shape	6-bundled	375	23.9	23.1	30	Whole
10	D-shape	6-bundled	375	23.9	23.1	45	Whole
11	D-shape	6-bundled	375	23.9	23.1	60	Whole
12	D-shape	6-bundled	375	23.9	23.1	75	Whole
13	D-shape	2-bundled	448	23.9	23.1	60	Sub-1
14	D-shape	2-bundled	448	23.9	23.1	60	Sub-2
15	D-shape	6-bundled	375	23.9	23.1	60	Sub-1
16	D-shape	6-bundled	375	23.9	23.1	60	Sub-2
17	D-shape	6-bundled	375	23.9	23.1	60	Sub-3

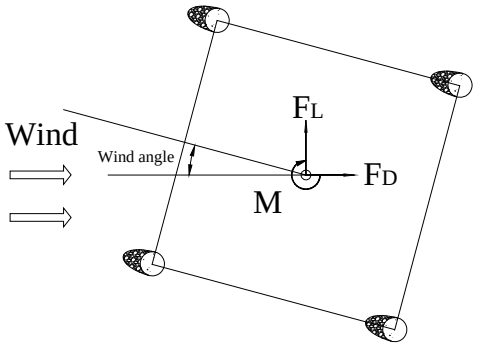

Fig. 2 Definition of aerodynamic force and wind angle for four-bundled crescent iced conductors

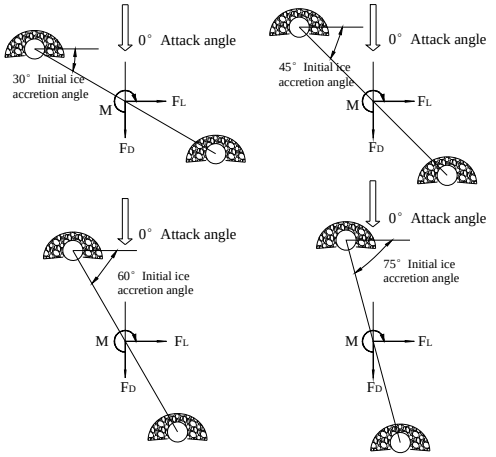

(a) Iced two-bundled conductor

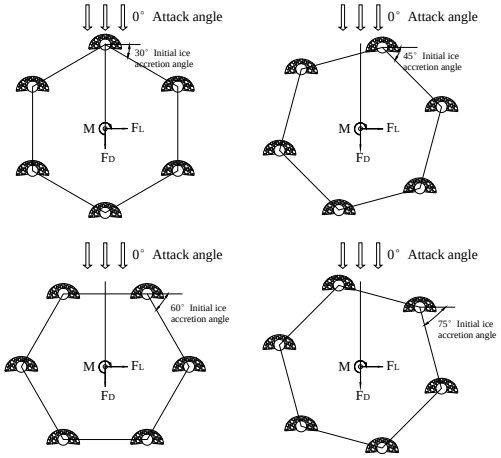

(b) Iced six-bundled conductor

Fig. 3 Definition of aerodynamic force and wind angle for D-shaped conductors with different initial ice accretion angle

Due to the wake interference of the iced bundled conductors, the aerodynamic characteristic of each sub-conductor may different from that of the single conductor case. As shown in Fig. 4, sub-conductors were numbered for two-bundled and six-bundled conductor models, respectively. Considering the symmetric arrangements of six-bundled conductors, only three sub-conductors were chosen to make measurement. A summary of test cases were given in Table 1 with parameter specifications. In the last column of Table, "Whole" indicates that the overall forces on a bundled conductor are measured by HFFB for the cases of 1 to 12; "Sub-1/2/3" indicates that only the aerodynamic forces on one single sub-conductor are measured for the cases of 13 to 17.

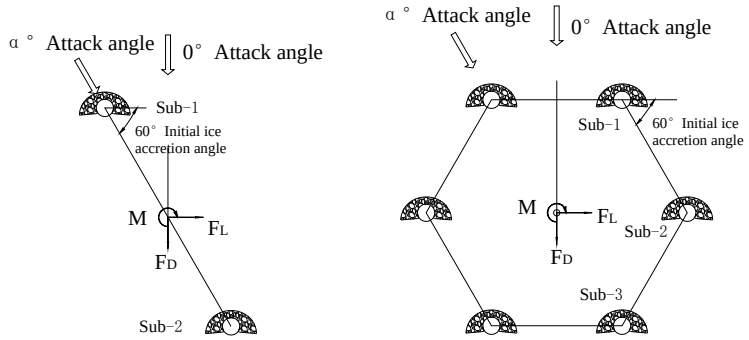

Fig. 4 Number of sub-conductors for D-shaped bundled conductors

2.3 Test facility and equipment

The wind tunnel tests were carried out in ZD-1 boundary layer wind tunnel, Zhejiang University. ZD-1 wind tunnel has a closed loop with a rectangular cross section, and the working cross section is 4 m (width)×3 m (height)×18 m (length). Its 1000 kW electrical engine allows a maximum wind speed up to 55m/s, and the minimum wind speed is about 3m/s. It was observed that the critical wind velocity which might cause galloping of iced conductors is about 7~15 m/s (CIGRE 2005). In this study, multiple spires at the entrance of the test section (as shown in Fig. 5) were used to simulate a typical homogeneous turbulent wind flow with a mean wind speed of 10 m/s and a 5% turbulence intensity. The use of 5% turbulence flow in the wind tunnel tests is due to the work of Lin (2012). Lin (2012) conducted the experiments for aerodynamic characteristics of single crescent conductor under three different flow conditions, i.e., the uniform flow, 5% turbulence intensity and 13% turbulence intensity. Lin concluded that the aerodynamic characteristic of conductor under 5% turbulence intensity is the most critical to cause galloping. Therefore, the authors selected 5% turbulence in this experiment study. High frequency force balance technique was employed to measure the aerodynamic forces of bundled conductors in crescent or D-shape with a sampling frequency of 200 Hz.

Two experimental setups were shown in Fig. 6. While Fig. 6(a) presents the setup for the test cases of 1 to 12 to measure the overall force on a bundled conductor, Fig. 6(b) shows the setup for the test cases of 13 to 17 for measuring aerodynamic forces on a single sub-conductor. The conductor model was rigidly connected with the balance through a transfer plate. The end plates with smooth surface were installed at the upper and lower ends of the conductor model to

eliminate the flow separation at the ends of the conductor. Thus, the simulated flow around the conductor model could be maintained as two-dimensional flow. There was a small gap between the top plate and the model to ensure that the wind load on the top plate would not be transferred to the conductor model. The bottom plate was raised up from the ground to eliminate the boundary layer effect of the wind tunnel. The attack angle was taken as 0°~180° for crescent conductors and 0°~360° for D-shape conductors with 5° intervals.

Fig. 5 Wind tunnel simulation of homogeneous turbulence and test models

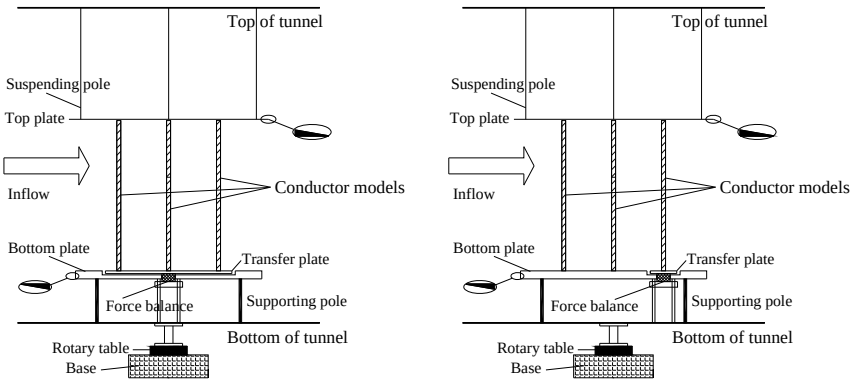

(a) Whole (b)Sub-conductor

Fig. 6 The experimental setup

3. Effects of ice thickness for crescent four-bundled conductors

3.1. Aerodynamic force coefficients

The main aerodynamic effects on iced conductors can be expressed in terms of drag, lift forces and moment. In this paper, the results of drag and lift forces were presented in terms of non-dimensional coefficients as follows

$$C_D^N(t) = \frac{1}{N}\frac{F_D(t)}{0.5\rho U^2 DH}, \qquad C_L^N(t) = \frac{1}{N}\frac{F_L(t)}{0.5\rho U^2 DH} \tag{1}$$

Where C_D and C_L are the drag and lift coefficients; F_D and F_L are the mean value of the measured drag and lift forces respectively; ρ is the air density of 1.225 kg/m³; U is the reference wind velocity of 10m/s; D is the diameter of the conductor and H is the length of the conductor model; N is the number of sub-conductors.

Fig. 7 shows the aerodynamic coefficients varying by attack angles in different ice thicknesses for crescent four-bundled conductors. The drag coefficient curves in Fig. 7(a) shows a half sine wave between 0° and 180° due to the change of the projecting area along the wind direction. For clearly showing the bundled effect, the drag and lift coefficient curves of a single conductor with 0.25D ice thickness were also provided in Fig. 7. For the case of a single conductor, the drag coefficient reaches the maximum value of 1.5 at the attack angle of 90°. But the peak of the drag coefficient curve around the angle of 90° was changed to be a valley for bundled conductors due to the bundled interference effects, in which the windward sub-conductor provides shields to the leeward sub-conductor such that the overall drag forces are reduced. The drag coefficients are larger for conductors with thicker accreted shapes within the range of large attack angles, i.e., from 25° to 155°.

Lift coefficients vary from positive to negative with the change of attack angles. It can be observed from the figure that crescent conductors with different ice thicknesses have similar aerodynamic lift curves just like full sine waves but with different amplitudes. The lift coefficients are 0 at 0° and 180° as the crescent ice section is symmetric. With the increase of ice thickness, the lift coefficients take larger and larger values resulting in two peaks emerge near the attack angles of 15° and 170°. While the overall maximum lift coefficient reaches at 2 for the conductor with 1D ice thickness under the attack angle of 15°, the local maximum value takes 0.5 for the conductor with 0.75D ice thickness around the angle of 170°. The bundled effect on the lift coefficients seems much smaller than that on the drag coefficients as shown in Fig. 7 (b), where two curves of lift coefficients almost coincides for the single conductor and four-bundled conductor with 0.25D ice thickness. The interference effects have been further discussed in section 5 for the case of D-shaped two and six bundled conductors.

3.2. Den Hartog coefficients

According to the Den Hartog instability mechanism, Den Hartog criterion may be expressed as a function of the aerodynamic coefficients of lift and drag and their derivatives as

$$Den = \frac{\partial C_L}{\partial \alpha} + C_D < 0 \tag{2}$$

where Den denotes the Den Hartog coefficient, and α is the wind attack angle. If Den is negative, the conductors would likely start to gallop.

As shown in Fig. 8, two unstable attack angle zones with negative Den Hartog coefficients can be identified for crescent four-bundled conductor. One is within the range of 15°~30°, and the other 170°~180°. With the decrease of ice thickness, the absolute value of the Den Hartog coefficient becomes smaller. For the ice thickness of 0.25D, the Den Hartog coefficients are all positive in the full range of attack angles. That is to say, according to the Den Hartog instability condition, the occurrence of galloping would be less possible for four-bundled conductors with thin ice coatings. The similar conclusion has also been reported in CIGRE (2005). Based on the results from wind tunnel tests and field observations, CIGRE (2005) claimed that ice accretions having a shape similar to an airfoil with significant thickness are more susceptible to experience Den Hartog instability.

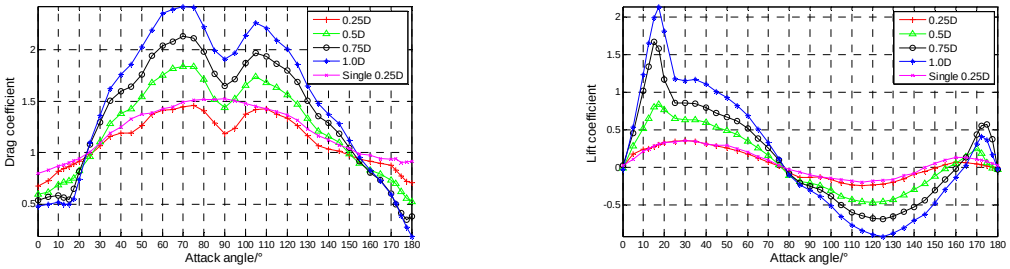

(a) Drag coefficient (b) Lift coefficient

Fig. 7 Aerodynamic coefficients of crescent four-bundled conductor

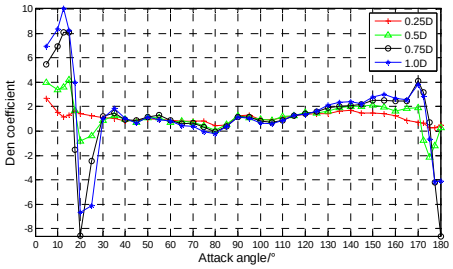

Fig. 8 Den Hartog coefficients of crescent-shaped four-bundled conductor

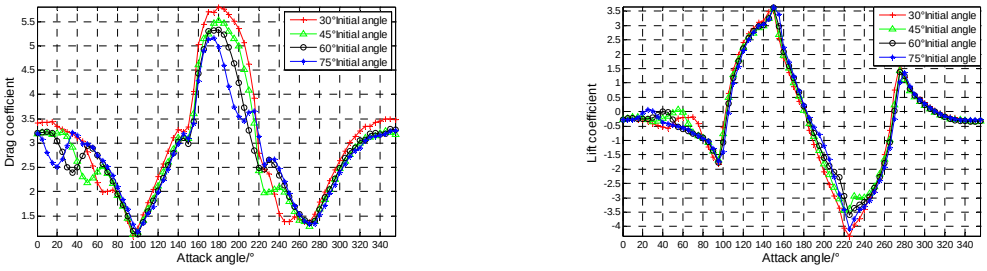

(a) Drag coefficient (b) Lift coefficient

Fig. 9 Aerodynamic force coefficients of D-shaped two-bundled conductors

4. Effects of initial ice accretion angle for D-shaped bundled conductors

As shown in Figs. 9 and 10, the change of initial ice accretion angle has a little influence to the lift coefficients, but does cause noticeable differences to the drag coefficients for D-shaped bundled conductors. Fig.11 shows the Den Hartog coefficients of D-shaped bundled conductors with various initial ice accretion angles. These curves show the same overall trend, and they are approximately symmetric about the wind attack angle of 180°. According to the Den Hartog criterion, galloping instability zones mainly exist in three ranges of wind attack angles, i.e., 60°~90°, 150°~225° and 280°~300°, for D-shaped bundled conductors.

Table 2 shows the wind attack angle ranges of galloping instability and their corresponding Den Hartog coefficients in different cases. As identified in Table 2, there is a large range of Den Hartog instability zone near 90°, 180° and 280° angles of attack. For D-shaped two-bundled conductors, the overall minimum value of Den Hartog coefficient is -8.5, which was observed for the case with an initial ice accretion angle of 75° within the wind attack angle ranges of 150°~225°. For D-shaped six-bundled conductors, the most critical Den Hartog instability zones also occur within the wind attack angle ranges of 150°~225°, corresponding to the minimum Den Harrog coefficient of -6 for the configuration with an initial ice accretion angle of 60°. The results indicates that relatively large ice accretion angels of 60° and 75° may cause most serious potential incidence of the Den Hartog instability condition, i.e., from 150° to 225° angles of attack for D-shaped bundled conductors.

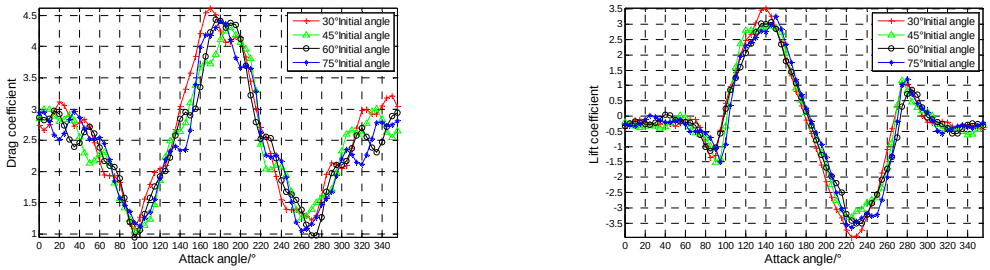

(a) Drag coefficient (b) Lift coefficient

Fig. 10 Aerodynamic force coefficients of D-shaped six-bundled conductors

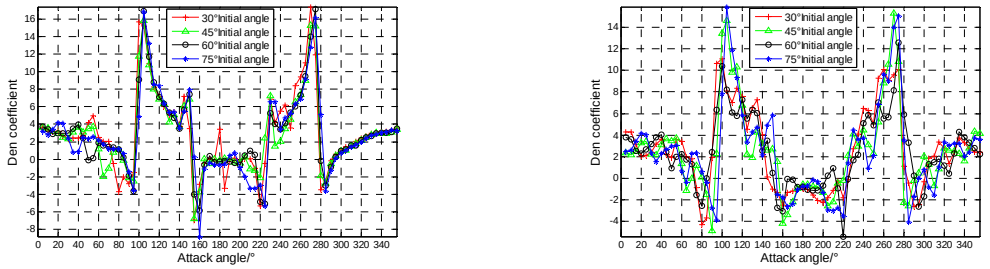

(a) Two-bundled conductors (b) Six-bundled conductors

Fig. 11 Den Hartog coefficients of D-shaped conductors

Table 2 Galloping instability zones and Den coefficients for D-shaped bundled conductors

Bundled	30° Initial ice angle		45°Initial ice angle		60°Initial ice angle		75°Initial ice angle	
	Attack angle/°	Den/min	Attack angle/°	Den/min	Attack angle/°	Den/min	Attack angle/°	Den/min
2	75~95	-3.5	60~95	-2.5	85~95	-3.5	85~95	-3.5
2	150~225	-7	150~225	-6.5	150~225	-5.5	150~225	-8.5
2	280~295	-3.5	280~295	-3	280~295	-3	280~295	-3.5
6	70~90	-4.5	65~95	-5.5	70~85	-2.5	65~95	-4
6	145~225	-2.5	155~220	-4	150~225	-6	155~220	-3.5
6	285~300	-2.5	280~290	-2.5	290~300	-2.5	280~310	-4

5. The interference effects of sub-conductors in D-shape

The differences in aerodynamic characteristics between single and bundled conductors have not been received adequate research. Due to interference effects, sub-conductors may have different aerodynamic characteristics compared to the isolated single conductors. In this study, aerodynamic forces acting on individual sub-conductors were measured under the configuration of 60° initial ice accretion angle for D-shaped two- and six-bundled conductors. Figs. 12 and 13 show the aerodynamic coefficients for sub-conductors of D-shaped two-bundled and six-bundled conductors, respectively. For comparison purpose, the aerodynamic coefficients of single conductor were collected from the previous wind tunnel test, in which only one single D-shaped conductor was tested (Lin 2012). The aerodynamic coefficients of single D-shaped conductor (denoted as “single”) and the aerodynamic coefficients of bundled conductors (denoted as “whole”, measured in case 7 and case 11) are also shown in the figures. It can be observed from Figs. 12 and 13 that the aerodynamic coefficient curve of single conductor seems much smoother than other curves, which show up some local fluctuations due to the interference effects of sub-conductors.

For sub-2 conductor of two-bundled conductors, the significant reduction of drag force was observed under the wind attack angle of 30° in Fig. 12. Under this attack angle, the shielding effect of sub-1 conductor to sub-2 conductor is significant such that the drag coefficient of sub-2 conductor was decreased by 1.5 from 3.5 at the attack angle of 10°. Therefore, a single conductor result cannot be used to explain the two-bundled conductor case. It is necessary to conduct wind tunnel tests to acquire aerodynamic force data for different configurations of bundled conductors in practice.

Due to the complex configuration of six-bundled conductors, the interference mechanism also becomes much more complicated compared to the case of two-bundled conductors. Therefore, as shown in Fig. 13, the aerodynamic coefficient curve of each sub-conductor experiences much more fluctuation. Fig. 14 gives the configuration of six-bundled conductors under the attack angle of 30°. In this configuration, sub-2 and sub-3 conductors were completely shielded by the upstream conductors, respectively. While the drag coefficient was decreased by 1 for sub-3

conductor, the reduction of drag coefficient was as much as 2.0 for sub-2 conductor. The difference in the reduction of drag by shielding can be attributed to the difference of clear spacing between sub-conductors and their upstream obstructions.

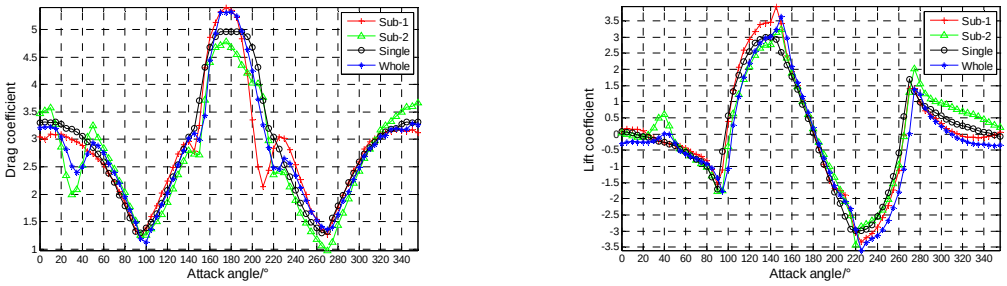

(a) Drag coefficient (b) Lift coefficient

Fig. 12 Aerodynamic coefficients of D-shaped two-bundled sub-conductors

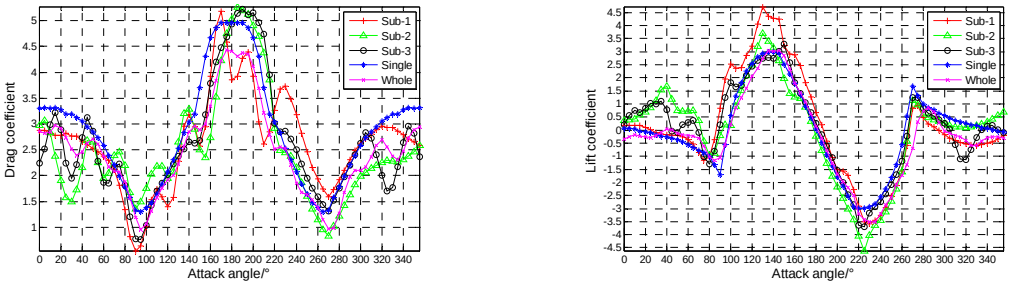

(a) Drag coefficient (b) Lift coefficient

Fig. 13 Aerodynamic coefficients of D-shaped six-bundled sub-conductors

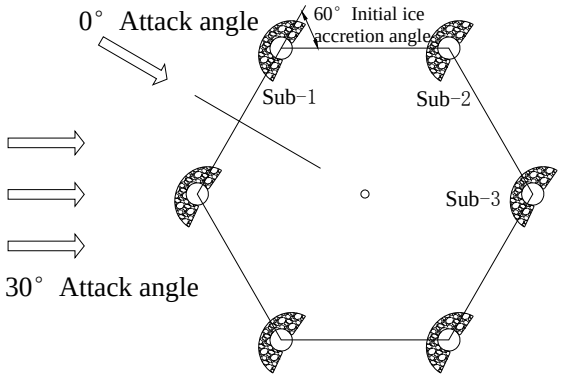

Fig. 14 Configuration of D-shaped six-bundled conductors under 30° attack angle

6. Galloping analysis of bundled conductors

6.1 Finite element models

One objective of the present work is to conduct galloping analysis of bundled conductors using the aerodynamic force data gathered in the wind tunnel tests. Since the aerodynamic force data was measured in a time history format by the high frequency force balance technique with a sampling frequency of 200 Hz, it becomes possible to simulate galloping in time domain by using the finite element model of an iced transmission line subjected to the measured aerodynamic forces.

Based on the work of Desai *et al*. (1995), a three-node parabola cable element can be used to model the conductor lines. The completely Lagrange form of the dynamic equilibrium equation of the cable element is given as

$$\boldsymbol{M}^e\ddot{\boldsymbol{q}}^e + \boldsymbol{C}^e\dot{\boldsymbol{q}}^e + {}_0^t\boldsymbol{K}^e\boldsymbol{q}^e = \boldsymbol{F}^e - \boldsymbol{Q}^e \tag{3}$$

$${}_0^t\boldsymbol{K}^e = {}_0^t\boldsymbol{K}_t^e + {}_0^t\boldsymbol{K}_\sigma^e \tag{4}$$

where $\boldsymbol{M}$ and $\boldsymbol{C}$ denote the mass matrix and damping matrix of a cable element, respectively; ${}_0^t\boldsymbol{K}^e$ denotes the tangent stiffness element matrix based on the initial form of the cable element ; $\boldsymbol{q}^e$ denotes nodal displacement vector, consisting of three translational components and one rotational component about the initial intrinsic axis of the cable; $\boldsymbol{F}^e$ is the external load vector, including aerodynamic force and gravity; $\boldsymbol{Q}^e$ is the unbalanced force vector of the cable element. As given in Eq. (4), the element stiffness matrix can be decomposed into linear elastic matrix ${}_0^t\boldsymbol{K}_t^e$ and the initial stress stiffening matrix ${}_0^t\boldsymbol{K}_\sigma^e$.

Each sub-conductors of bundled conductor are connected to each other by spacers. The finite element model of six-bundled conductors is shown in Fig. 15. The spacer can be modeled by the Euler beam element. The displacement vector ${}_0^t\boldsymbol{q}_B$ of a beam element is given in terms of six displacement components reference to the Global coordinate system as

$${}_0^t\boldsymbol{q}_B = [\,{}_0^t\boldsymbol{q}_{B,i} \quad {}_0^t\boldsymbol{q}_{B,j}\,]^{\mathrm{T}} \tag{6}$$

$${}_0^t\boldsymbol{q}_{B,k} = [\,{}_0^tu_k \quad {}_0^tv_k \quad {}_0^tw_k \quad {}_0^t\theta_{x,k} \quad {}_0^t\theta_{y,k} \quad {}_0^t\theta_{z,k}\,]^T \qquad k=i,\ j \tag{7}$$

While the beam element has three translational freedoms and three torsion freedoms, the cable element modeling conductors has three translational freedoms and one torsion freedom. It is critical to ensure the compatibility of the common node connecting the cable element of conductors and the beam element of spacers. By introducing a freedom reduction matrix ${}^t\boldsymbol{R}$, the three torsion freedoms of a beam element can be reduced into one torsion freedom about the cable element, which share a common node with the beam element. The displacement vector ${}_0^t\boldsymbol{q}_{BR}$ for the beam element after freedom reduction can be expressed as

$${}_0^t\boldsymbol{q}_{BR} = {}^t\boldsymbol{R}\,{}_0^t\boldsymbol{q}_B = [\,{}_0^t\boldsymbol{q}_{BR,i} \quad {}_0^t\boldsymbol{q}_{BR,j}\,]^{\mathrm{T}} \tag{8}$$

$${}_0^t\boldsymbol{q}_{BR,k} = [\,{}_0^tu_k \quad {}_0^tv_k \quad {}_0^tw_k \quad {}_0^t\theta_{S,k}\,] \qquad k=i,\ j \tag{9}$$

where the freedom reduction matrix is written as

$$ {}^{t}\boldsymbol{R} = \begin{bmatrix} \boldsymbol{I}_{3\times3} & \boldsymbol{O}_{3\times3} & \boldsymbol{O}_{3\times3} & \boldsymbol{O}_{3\times3} \\ \boldsymbol{O}_{1\times3} & {}^{t}\boldsymbol{R}_{i} & \boldsymbol{O}_{1\times3} & \boldsymbol{O}_{1\times3} \\ \boldsymbol{O}_{3\times3} & \boldsymbol{O}_{3\times3} & \boldsymbol{I}_{3\times3} & \boldsymbol{O}_{3\times3} \\ \boldsymbol{O}_{1\times3} & \boldsymbol{O}_{1\times3} & \boldsymbol{O}_{1\times3} & {}^{t}\boldsymbol{R}_{j} \end{bmatrix}_{8\times12} \tag{10} $$

$$ {}^{t}\boldsymbol{R}_{k} = [\cos\alpha_{k}^{t} \quad \cos\beta_{k}^{t} \quad \cos\gamma_{k}^{t}] \qquad k=i, j \tag{11} $$

in which ${}_{0}^{t}\alpha_{k}$、${}_{0}^{t}\beta_{k}$ and ${}_{0}^{t}\gamma_{k}$ are the angles between tangential direction of the cable element and each axis, respectively. $\boldsymbol{I}$ is the unit matrix and $\boldsymbol{O}$ is the zero matrix. It is worth noting that the use of freedom reduction technique can significantly improve the overall computational efficiency for numerical galloping simulation of bundled conductors.

6.2. Wind loads on bundled conductors

The aerodynamic forces acting on the iced D-shape conductor can be expressed as

$$ [F_y \ F_z \ M]^{\mathrm{T}} = \frac{1}{2}\rho_{air}U_z^2 D[C_y(\alpha) \ C_z(\alpha) \ DC_M(\alpha)]^{\mathrm{T}} \tag{12} $$

$$ \begin{aligned} C_y &= C_L\cos\alpha - C_D\sin\alpha \\ C_z &= C_L\sin\alpha + C_D\cos\alpha \end{aligned} \tag{13} $$

where ρ_{air} denotes the air density, D denotes the conductor diameter, U_z denotes the mean wind velocity; C_L、C_D and C_M denote the lift, drag and moment coefficients, which depend on the ice shape and wind attack angle α

$$ \alpha = \beta + \theta - \frac{\dot{y}}{U_z} - \frac{D\dot{\theta}}{2U_z} \tag{14} $$

in which β is the initial wind attack angle, θ is the torsion angle at time t, as depicted in Fig. 16. The aerodynamic force coefficients were obtained from the wind tunnel tests for iced conductors.

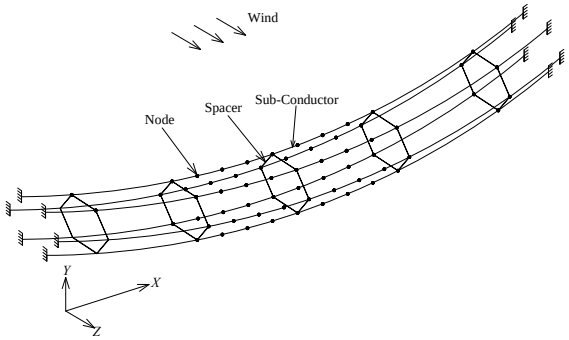

Fig. 15 Finite element model of bundled conductors

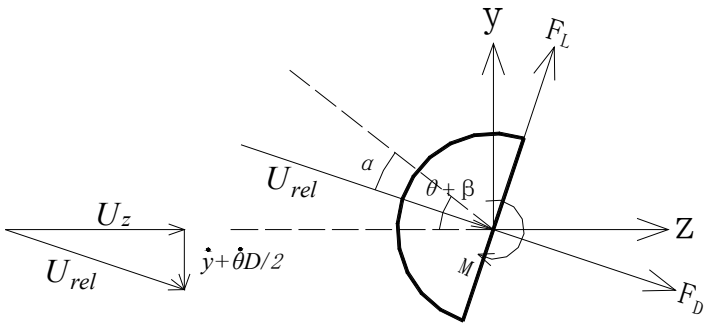

Fig. 16 Attack angle and aerodynamic forces of iced D-shape conductor

6.3. Time history solutions

Numerical simulation for galloping analysis was performed considering a practical transmission line with a span of 244 m used for state UHV grids of China. The iced conductor used in the transmission line is D-shape six-bundled conductors with an initial ice accretion angle of 60° and parameters provided in Table 3. Two load cases are simulated that are described as: Example A) Making use of the aerodynamic force measured for each sub-conductor corresponding to the test cases of Nos. 15-17 in Table 1; Example B) Making use of the aerodynamic force measured as a whole for D-shape six-bundled conductors corresponding to the test case of No. 11 in Table 1. According to the galloping instability zones identified in Table 2, wind attack angle of 150° was chosen for galloping analysis. Galloping was observed at a wind speed, normal to the span, of about 12 m/s so that the same value was employed in the computer simulation.

The galloping responses of D-shape 6-bundled conductors at the middle of the span were shown in Fig. 17 for horizontal displacements and Fig. 18 for vertical displacements, respectively. Due to the symmetric arrangements of sub-conductors in Fig. 14, only the results of three sub-conductors of Example A have been discussed here. As shown in Fig. 17(a), three sub-conductors of Example A and the whole bundled conductors of Example B have the similar time history trends in the horizontal displacements. While three sub-conductors reach their maximum vibration amplitudes almost at the same time instant of 120 s, the whole bundled conductors of Example B start to be in full vibration amplitude at a much earlier time instant of 60 s. In the developed vibration stage, i.e., the time duration of 140 s to 160 s as shown in Fig. 17(b), there are slight differences in the total displacement range and the vibration phase between sub-conductors of Example A and the whole bundled conductor of Example B. The whole bundled conductor behavior as a sine wave with a shifted phase and a smaller negative peak of -3 m compared to the vibration curves of sub-conductors. In terms of galloping amplitude, Fig. 17 shows the final stable magnitude is no more than doubling compared to the initial oscillation amplitude. Such a result indicates that the horizontal galloping response shown in Fig. 17 is less significant compared to the vertical response presented in Fig. 18.

For vertical displacement, there are noticeable differences between Example A and Example B both in full time response histories and the developed vibration stage. The full-time variation patterns of three sub-conductors in Fig. 18(a) clearly show asymmetric features about their mean amplitudes. In the developed vibration stage as shown in Fig. 18(b), the vibration curves of three

sub-conductors also become distinguishable from each other, particularly at the local peak positions. The variation of vertical response seems much more significant than the horizontal galloping response. The asymptotic amplitude along the vertical direction reaches 4 m almost four times of the 1 m initial amplitude. The obvious amplification of oscillation amplitude during galloping is also confirmed by the field observation (CIGRE 2005), and is of practical concern.

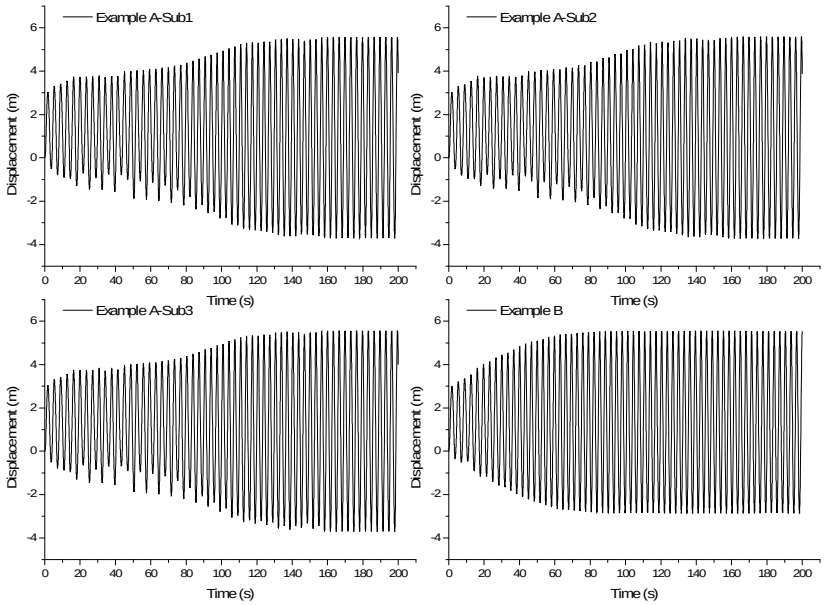

(a) Response in full-time duration

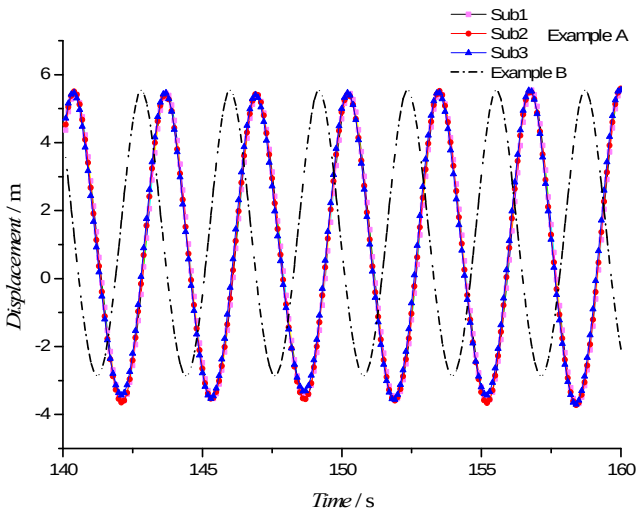

(b) Response in time duration of 140s to 160s

Fig. 17 Horizontal galloping response of D-shape 6-bundled conductors

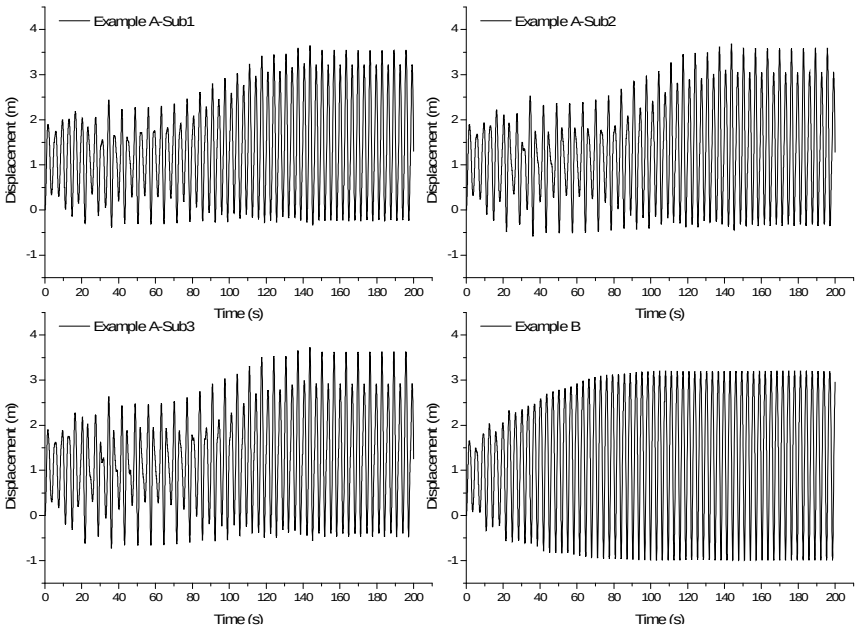

(a) Response in full-time duration

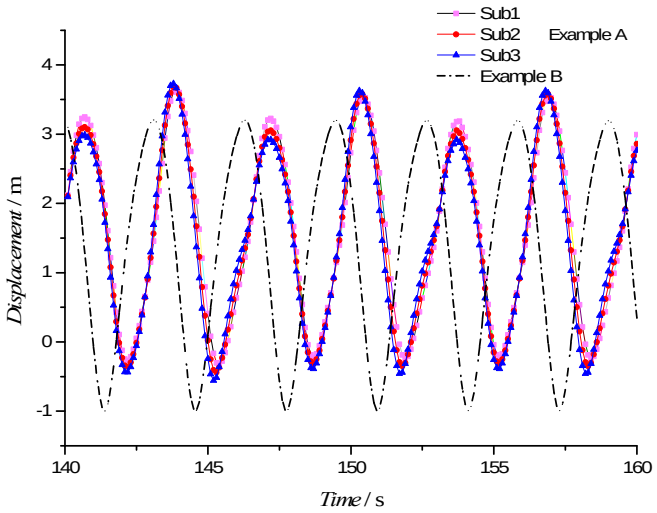

(b) Response in time duration of 140 s to 160 s

Fig. 18 Vertical galloping response of D-shape 6-bundled conductors

Fig. 19 presents power spectral densities of horizontal and vertical galloping responses. While the whole conductor responses of Example B are mainly dominated by one single spectral peak at a frequency value of 0.3 Hz, several energy peaks at three distinctive frequency points contribute to the galloping responses of sub-conductors of Example A. Such an energy constitution of

multiple resonant frequency points causes the asymmetric time-domain patterns (tend to be random) of galloping responses for sub-conductors of Example A.

Table 3 Physical parameters of iced six-bundled conductors

Parameter	Symbol	Unit	Value
Axial stiffness	AE	10^6N	27.64
Torsional stiffness	GJ	Nm^2/rad	291.46
Horizontal tension	H	10^3N	41.65
Conductor diameter	d	10^{-3}m	26.82
Span	L_x	m	244.00
Height difference of support	h	m	0
Linear density of conductor	ρ	kg/m	1.349
Linear density of accretion ice	ρ_{ice}	kg/m	0.85
Rotational inertia of unit length	I_o	10^{-4} kg m^2/m	6.40

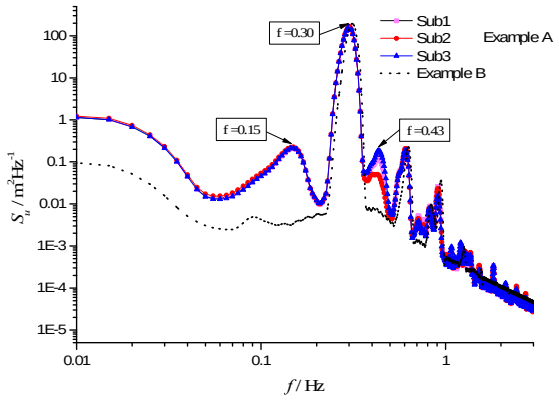

(a) Horizontal galloping responses

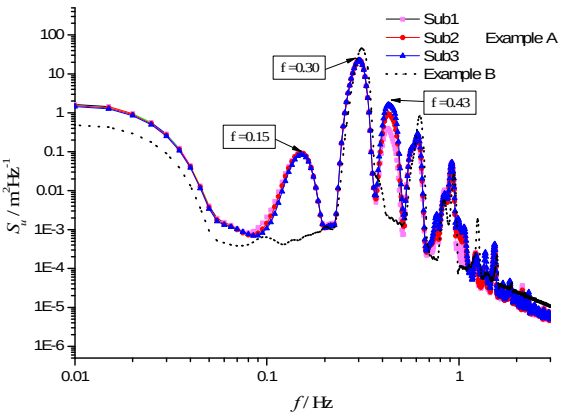

(b) Vertical galloping responses

Fig. 19 Power spectral densities of galloping responses of D-shape 6-bundled conductors

7. Conclusions

Wind tunnel tests using high frequency force balance technique have been carried out to acquire the aerodynamic force coefficients of crescent two-bundled, D-shape two-bundled and D-shape six-bundled conductors. A systematical research was performed to reveal the influence of the ice thickness and the initial ice accretion angle on the aerodynamic characteristics of crescent and D-shape bundled conductors. The interference effects of sub-conductors were also investigated for D-shape two-bundled and six-bundled conductors by measuring aerodynamic forces of sub-conductors. The potential incidences of the Den Hartog instability condition for iced bundled conductors have been identified. There are two Den Hartog instability zones, i.e., 15°~30° and 170°~180°, for iced four-bundled conductors in crescent shapes. D-shape bundled conductors have a large range of galloping instability covering three zones of wind attack angles, i.e., 60°~90°, 150°~225° and 280°~300°. Based on the measured aerodynamic force coefficients, galloping behavior of a D-shape six-bundled conductor with a span of 244 m were successfully simulated by a finite element model. The results demonstrate that sub-conductors have different galloping response patterns when aerodynamic force coefficients of sub-conductors considering interference effects were used in the analysis.

Acknowledgements

The work described in this paper was partially supported by the National Natural Science Foundation of China (Project Nos. 51178424 and 51378468).

References

Barrero, A., Sanz, A. and Alonso, G. (2009), "Hysteresis in transverse galloping: the role of the inflection points", *J. Fluid. Struct.*, **25**, 1007-1020.

Chabart, O. and Lilien, J.L. (1998), "Galloping of electrical lines in wind tunnel facilities", *J. Wind Eng. Ind. Aerod*., **74**, 967-976.

CIGRE. (2005), State of the art of conductor galloping. TB (Technical Brochure), Task Force B2.11.06, December. Convenor, SCB2 WG11.

Den Hartog, J.P. (1932), "Transmission line vibration due to sleet", *Am. Inst. Elec. Engineers, T.*, **51**(4), 1074-1076.

Desai Y.M., Yu, P., Popplewell, N. and Shah, A.H. (1995), "Finite element modeling of transmission line galloping", *Comput. Struct.*, **57**(3), 407-420.

Gu, M., Ma, W. and Quan, Y. (2009), "Aerodynamic Force Characteristics and stabilities of Two Typical Iced Conductors", *J. Tongji University (Natural Science)*, **37**(10), 1328-1332.

Guo, Y., Li, G. and You, C. (2002), *Galloping of electrical transmission line*, China Electric Power Press, Beijing.

Jones, K.F. (1992), "Coupled vertical and horizontal galloping", *J. Eng. Mech .- ASCE*, **118**(1), 92-107.

Li, Y., Wu, M., Chen, X., Wang, T. and Liao, H. (2013). "Wind-tunnel study of wake galloping of parallel cables on cable-stayed bridges and its suppression", *Wind Struct.*, **16**(3), 249-261.

Lin, W. (2012), *Wind tunnel and numerical study on aerodynamic characteristics of ice accreted transmission lines*, Master thesis, Zhejiang University, Hangzhou.

Lv, Y., Lou, W., Sun, Z. and Li, H. (2010), "Numerical simulation of aerodynamic characteristics of three bundled iced transmission lines", *J. Zhejiang University (Engineering Science)*, **44**(1), 174-179.

Luongo, A., Zulli, D. and Piccardo, G. (2008), "Analytical and numerical approaches to nonlinear galloping of internally resonant suspended cables", *J. Sound Vib.*, **315**, 375-393.
Luongo, A., Zulli, D. and Piccardo, G. (2009), "On the effect of twist angle on nonlinear galloping of suspended cables", *Comput. Struct.*, **87**, 1003-1014.
Macdonald, J.H.G. and Larose, G.L. (2006), "A unified approach to aerodynamic damping and drag/lift instabilities, and its application to dry inclined cable galloping", *J. Fluid. Struct*., **22**(2), 229-252.
Nigol, O. and Buchan, P.G. (1981), "Conductor galloping-part II Torsional mechanism", *Power Apparatus Syst., IEEE T.* (2), 708-720.
Ohkuma, T. and Marukawa, H. (2000), "Galloping of overhead transmission lines in gusty wind", *Wind Struct.*, **3**(4), 243-253.
Parkinson, G. (1989), "Phenomena and modeling of flow-induced vibrations of bluff bodies", *Prog. Aerosp. Sci.*, **26**(2), 169-224.
Raeesi, A., Cheng, S. and Ting, D.S.K. (2013), "Aerodynamic damping of an inclined circular cylinder in unsteady flow and its application to the prediction of dry inclined cable galloping", *J. Wind Eng. Ind. Aerod.*, **113**, 12-28.
Shimizu, M., Ishihara, T. and Phuc, P.V. (2004), "A wind tunnel study on aerodynamic characteristics of ice accreted transmission lines", *Proceedings of the 5th International colloquium on bluff body aerodynamics and applications*.
Sun, Z. and Lou, W. (2010), "Nonlinear finite element analysis on galloping of ice-coated transmission line", *Power Syst. Technol.*, **34**(12), 214-218.
Van Dyke, P. and Laneville, A. (2008), "Galloping of a single conductor covered with a D-section on a high-voltage overhead test line", *J. Wind Eng. Ind. Aerod.*, **96**(6), 1141-1151.
Wang, X., Lou, W. J., Shen, G.H. and Xu, F.Y. (2011), "A wind tunnel study on aerodynamic characteristics of iced conductor", *Acta Aerod.Sinica*, **5**(29), 573-579.
Wang, X. and Lou, W. (2010), "Numerical approach to the gallop of iced conductor", *Eng. Mech.*, **1**(27), 290-293.
Xiao, Z., Yan, Z., Li, Z., Wang, Z. and Huang, H. (2009), "Wind tunnel and aerodynamic characteristics tests for ice-covering of transmission line adopting 8-bundled conductor", *Power Syst. Technol.*, **33**(5), 90-94.
Yan, Z., Yan, Z., Li, Z. and Tan, T. (2013), "Nonlinear galloping of internally resonant iced transmission lines considering eccentricity", *J. Sound Vib.*, **331**, 3599-3616.
Yu, P., Shah, A.H. and Popplewell, N. (1992), "Inertially coupled galloping of iced conductors", *J. Appl.Mech. -T ASME*, **59**, 140-145.
Yu, P., Desai, Y.M., Shah, A.H. and Popplewell, N. (1993), "Three-degree-of-freedom model for galloping. Part I: formulation", *J. Eng. Mech.*, **119**(12), 2404-2425.

CC